

TRANSITION REGION DOWNFLOWS IN THE IMPULSIVE PHASE OF FLARES

S. Kamio, H. Kurokawa, and D. H. Brooks

Kwasan and Hida Observatories, Kyoto University, Kyoto 607-8471, Japan, Email:kamio@kwasan.kyoto-u.ac.jp

ABSTRACT

We present observations of 4 flares which occurred during coordinated observations between Coronal Diagnostic Spectrometer (CDS) on board SOHO and Domeless Solar Telescope at Hida Observatory(DST/Hida). We studied the evolution of flare kernels using H α images of DST/Hida, and derived Doppler velocities from high time cadence (42 sec) SOHO/CDS data. Downflows are detected in the chromosphere and transition region temperature range during the impulsive phase of the flares. Downflows in the chromosphere have been reported in previous papers, and they have been interpreted as chromospheric evaporation process. Our results suggest that these downflows in the transition region are a common characteristic of flares. They are important for understanding the dynamics of the solar atmosphere in response to the sudden energy deposition of a flare.

Key words: Sun: UV radiation — Sun: transition region — Sun: chromosphere.

1. INTRODUCTION

Chromospheric evaporation is believed to be responsible for sudden increases in H α and soft X-ray emissions during the impulsive phase of flares. According to the chromospheric evaporation scenario, high energy particles generated in the flare flow along the magnetic field and penetrate into the dense plasma of the chromosphere. This leads to explosive heating of the plasma up to 10^7 K, and the explosion in the magnetic flux tube produces both upflow and downflow of the heated plasma, which should be observable at different temperatures in the solar atmosphere. Chromospheric evaporation was first proposed by Neupert (1968), and upflows and downflows during the impulsive phase of flares have been reported in previous papers.

Ichimoto and Kurokawa (1984) detected red asymmetry emission in H α spectra during a flare, which was identified as a downflow of 50-100km/s in the chromosphere(10^4 K). Antonucci et al. (1982) found blue-shifted component in Ca XIX and Fe XXV spectra obtained with SMM/BCS during the impulsive phase, and derived upflow velocities of 300-400 km/s. Strong upflows in the plasma of 10^7 K during the impulsive phase of flares support the chromospheric evaporation model. Wülser et al. (1994) studied GOES X1.5 flare on 15 November 1991, which was observed by the Yohkoh satellite and the Mees Solar Observatory. They analysed Ca XIX spectra obtained with Yohkoh/BCS (Culhane et al., 1991) and detected an upflow component of 250km/s during the impulsive phase of the flare. They

also found red shifts of 19-42km/s in H α spectrum, and claimed that the estimated momenta of upflow and downflow were balanced.

In the transition region around 10^5 K, upflows and downflows have been reported in previous studies. Cheng et al. (1986) derived the velocity and density variation in the transition region using Si IV and O IV lines (8×10^4 K). They found downflows up to 20km/s and density increases of a factor 3 during the impulsive phase. However, wavelength scanning of UVSP instrument on board SMM caused some ambiguity in the velocity determination during the rapidly changing flare. Brosius (2003) studied the evolution of an M6.3 flare on 15 June 2001 observed with SOHO/CDS (Harrison et al., 1995). He detected a 360km/s upflow component and a 50km/s downflow component simultaneously in O V ($\log T = 5.4$) during the impulsive phase of the flare. But the spatial distribution of the flare was not apparent because his data were sit-and-stare observation. Teriaca et al. (2003) analysed a C1.1 flare on 26 May 2001 using SOHO/CDS and a spectroheliograph at the Dunn Solar Telescope. They found oppositely directed flows in the same flare kernel at the beginning of the flare. Derived velocities were 30 ~ 40km/s downward for He I 10830Å, 100 km/s upward for O V, and 20 ~ 160 km/s upward for FeXIX($\log T = 6.9$). However, the temporal evolution during the flare was not clear, because their time cadence was about 5 min.

We present observations of several flares which occurred during coordinated observation with SOHO/CDS and Domeless Solar Telescope(DST) at Hida Observatory. Our observations are characterized by high time cadences, which are 42s for SOHO/CDS and 15s for DST H α images, and simultaneous coverage of the chromosphere, transition region, and corona. Although the CDS cadence is lower than Brosius (2003), we obtained wider spatial coverage (through raster observations) which are necessary for coalignment with the DST images.

2. OBSERVATIONS

Coordinated observations between Hida/DST and SOHO/CDS were carried out from 26 July to 9 August in 2002. In the DST, H α images were obtained with a Lyot filter of 0.25Å FWHM. The filter wavelength was shifted in the sequence of -0.8, -0.5, +0.0, +0.5, and +0.8Å from H α line center, and the time cadence was 15 sec for each wavelength. The spatial resolution was 0.5 at its best, though it varied with the seeing conditions.

The SOHO/CDS program was designed to achieve a high time cadence of 42 sec while retaining some spatial cov-

erage. We used the normal incidence spectrometer (NIS) 4×240 slit and scanned an area of 16×240 . Wide field scans of 48×240 were taken every 50 scans, which were used for co-alignment with the DST $H\alpha$ images. Data were binned in the y-direction along the slit for the sake of high time resolution, and the spatial resolution after binning was 4×3.2 . We selected the spectral lines He I $\lambda 584.33$ ($\log T_e = 4.55$), O V $\lambda 629.73$ (5.35), and Mg IX $\lambda 368.06$ (6.00), covering the temperature ranges of the upper chromosphere, transition region, and corona. These lines are amongst the strongest in the NIS spectra and are therefore suitable for high cadence studies.

During this observational campaign, 4 flares were simultaneously observed by the DST and CDS. In this paper, we present the results for the flare on 7 August 2002 and 31 July 2002 which were the smallest (GOES B7.7) and the largest (M1.2) among 4 flares.

3. RESULTS

A B7.7 flare occurred in active region NOAA 10061 at 23:43 UT on 7 August 2002. Our observations started at 22:29 UT, so the preflare and impulsive rise of the flare were captured with CDS and the DST. The $H\alpha$ filter image with an overlying contour of the He I intensity map is presented in Fig. 1. 5 flare kernels were identified in the sequence of $H\alpha$ line center images, which are labeled A-E in Fig. 1. Since $H\alpha$ kernel B was in the field of view of CDS, the evolutions of kernel B is studied in detail.

Fig. 3 shows the temporal evolution of kernel B. GOES soft X-ray flux is presented in the upper panel. The time derivative of the GOES soft X-ray flux is used as a proxy for the hard X-ray flux (Neupert, 1968). It showed a main peak at 23:43 UT and a less intense peak at 23:41 UT. We also plotted 17GHz microwave flux from the active region obtained with Nobeyama Radio Heliograph (NoRH; Nakajima et al. 1994). In view of chromospheric evaporation, hard X-ray peaks indicate energy deposition at the foot points of magnetic loops, and the soft X-ray flux represents the amount of evaporated plasma (10^7 K). Microwave bursts are thought to be produced by non-thermal electrons generated in the flare. These light curves suggest that the main energy release of the flare occurred at 23:43 UT.

The middle panel in Fig 3 shows the light curves of CDS He I, O V, and Mg IX. Note that the intensity peaks in He I and O V coincided with the soft X-ray time derivative and the microwave burst at 23:43 UT. This implies that these brightenings are directly related to the energy deposition into the chromosphere and transition region. The bottom panel in Fig 3 presents the relative Doppler velocities derived from CDS spectra. Because the CDS can not measure absolute wavelength, we inferred relative velocities on the assumption that the average velocities are 0. We corrected systematic trend by using detailed data reduction procedure developed and described by Brooks and Kurokawa (2004). Downflow velocities are detected in He I (15 km/s) and O V (80 km/s) at 23:43 UT, which

coincided with the intensity peaks. These velocities in He I and O V exceeded 3σ levels and are significant, but no significant velocity was found in Mg IX.

We also studied M1.2 flare on 31 July 2002 in the same way. Fig. 2 shows $H\alpha$ image with overlaid contour of CDS He I. Two flare ribbons were found in the opposite polarity regions, and 3 $H\alpha$ kernels were located in the CDS field of view. Light curves and the velocities at kernel A is presented in Fig. 4. Downflows of 30 km/s were detected in He I and O V at 01:42 UT. The O V downflows increased to 80km/s by 01:46 UT which coincided with O V intensity peak. In He I, smaller but significant (3σ level) velocity was detected at the same time. In the velocity curve of O V from 01:41 UT to 01:49 UT, 3 peaks are found at 01:42 UT, 01:46 UT, and 01:48 UT. These peaks coincided with soft X-ray time derivative peaks in the upper panel, and this suggests that these downflow motions consisted of at least 3 short-lived events in kernel A.

4. SUMMARY AND DISCUSSION

Flare dynamics are important for understanding energy release and transport in the solar atmosphere. Previously, downflows in the chromosphere during the impulsive phase have been reported in several papers (e.g. Ichimoto and Kurokawa 1984). Very recent observation of one event also indicated the presence of downflows in the transition region (Brosius and Phillips, 2004). We found short-lived (less than 2 min) downflows in O V and He I during the impulsive phase. Our results suggest that downflows in the transition region may be a common characteristic of the flare impulsive phase, regardless of flare size, and that they are related to the chromospheric evaporation process. More detailed analysis of all 4 flares will be presented in the forthcoming paper.

Our result show that high time cadence is necessary for the detailed study of the chromospheric evaporation process. CDS observational program was aimed at high time cadence (42s), but high speed downflows were detected in only one exposure. The field of view was narrow since we chose high time resolution for the CDS, however, the combination of imager and spectrometer allow us to obtain both spatial and spectral information in high time cadence, which are important for the flare study.

Solar-B, scheduled to be launched on 2006, will allow us to measure more accurate Doppler velocity (± 3 km/s) with EUV Imaging Spectrometer (EIS). We will be able to study the dynamics in a flare kernel more precisely with high spatial resolution of EIS (pixel size of 1 arcsec). Spectroscopic observations of the chromospheric lines are necessary to investigate the detailed evolution in the chromosphere. Previously several papers have been published on that subject, however, simultaneous spectroscopy of the chromosphere, the transition region, and the corona will bring us better understanding of the chromospheric evaporation and energy transport in the solar atmosphere.

ACKNOWLEDGMENTS

We would like to thank A. Fludra for his help in planning and executing the CDS observations. CDS was built and is operated by a consortium led by Rutherford Appleton Laboratory and including Mullard Space Science Laboratory, the NASA Goddard Space Flight Center, Oslo University, and the Max Planck Institute for Extraterrestrial Physics, Garching. *SOHO* is a mission of international cooperation between ESA and NASA.

REFERENCES

- Antonucci, E., Gabriel, A. H., Acton, L. W., Culhane, J. L., Doyle, J. G., Leibacher, J. W., Machado, M. E., Orwig, L. E., and Rapley, C. G., *Sol. Phys.*, 78, 107, 1982.
- Brooks, D. H. and Kurokawa H. , *ApJ*, 611, 1125, 2004.
- Brosius, J. W. , *ApJ*, 586, 1417, 2003.
- Brosius, J. W. and Phillips, K. J. H, *ApJ* preprint doi:10.1086/422873, 2004.
- Cheng, C. -C. and Tandberg-Hassen, E. *ApJ*, 309, 421, 1996.
- Culhane, J. L., Bentley, R. D., Hiei, E., Watanabe, T., Doschek, G. A., Brown, C. M., Cruise, A. M., Lang, J., Ogawara, Y., and Uchida, Y., *Sol. Phys.*, 136, 89, 1991.
- Harrison, R. A. et al. *Sol. Phys.*, 162, 233, 1995.
- Ichimoto, K. and Kurokawa, H., *Sol. Phys.*, 93, 105, 1984.
- Nakajima, H., et al., *Proc. of the IEEE*, 82, 705, 1994.
- Neupert, W. M., *ApJL*, 153, 59, 1968.
- Teriaca, L., Falchi, A., Cauzzi, G., Falciani, R., Smaldone, L. A., and Andretta, V., *ApJ*, 588, 596, 2003.
- Wülser, J.-P., Canfield, R.C., Acton, L.W., Culhane, J. L., Phillips, A., Kosugi, T., and Tsuneta, S. , *ApJ*, 424, 459, 1994.

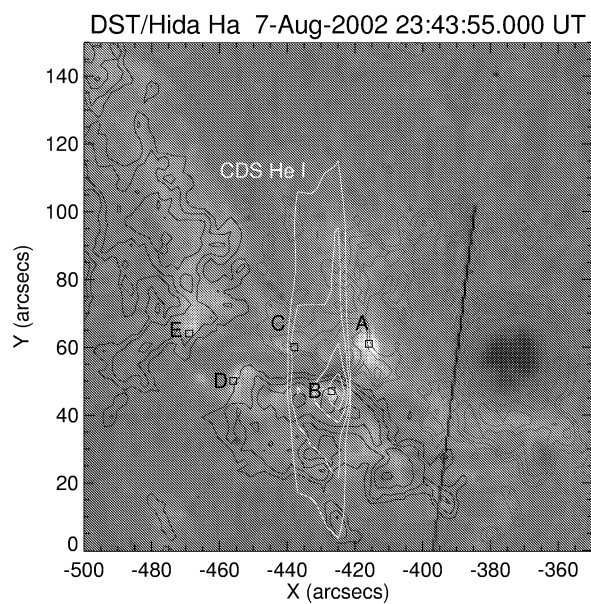


Figure 1. $H\alpha$ image in the impulsive phase of the flare on 7 August 2002 with overlaid contours of CDS He I intensity map (yellow contours). Red and blue contours indicate positive and negative magnetic field on the photosphere obtained with SOHO/MDI.

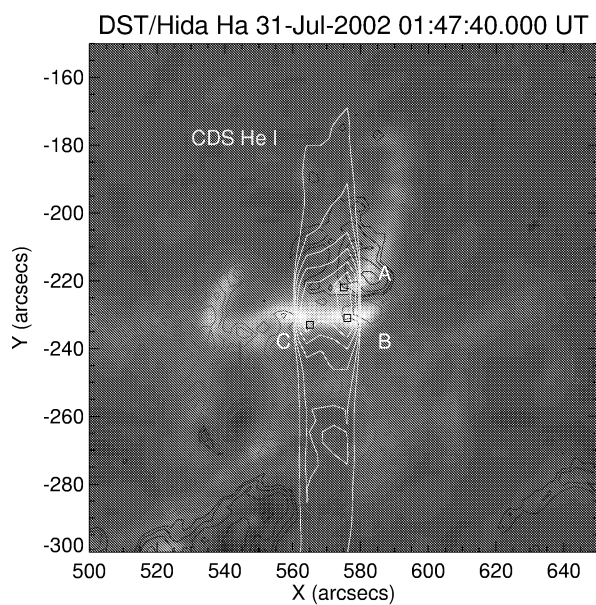


Figure 2. Same as Fig.1, but for the flare on 31 July 2002.

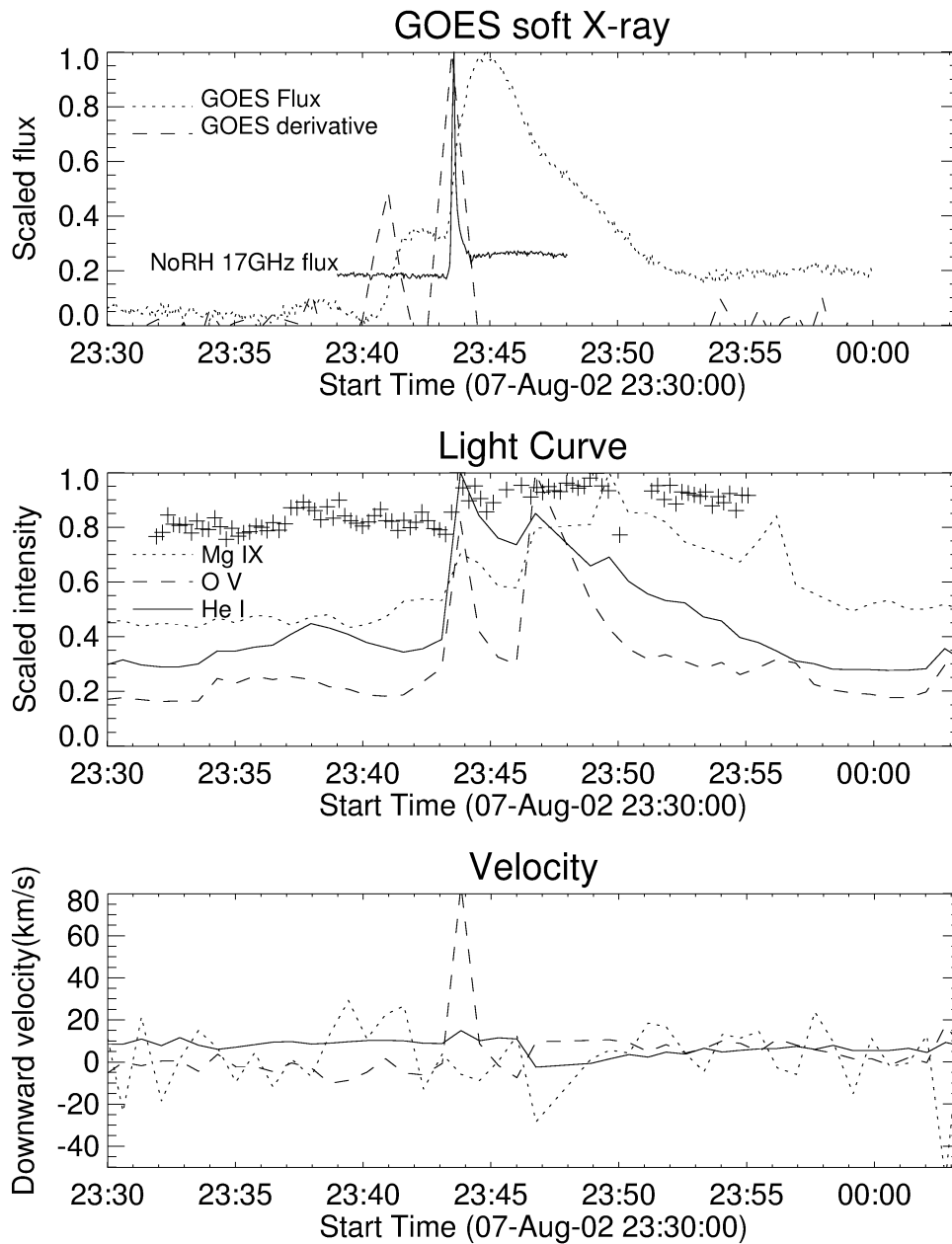


Figure 3. Temporal evolution of the flare kernel B in Fig. 1. Upper panel: GOES soft X-ray flux (dotted), the time derivative of soft X-ray (dashed), and 17GHz microwave flux in the active region (solid). Middle panel: Normalized light curves of CDS He I (solid), O V (dashed), and Mg IX (dotted). Plus signs indicate H α intensity at kernel B. Lower panel: Doppler velocities derived from CDS spectra.

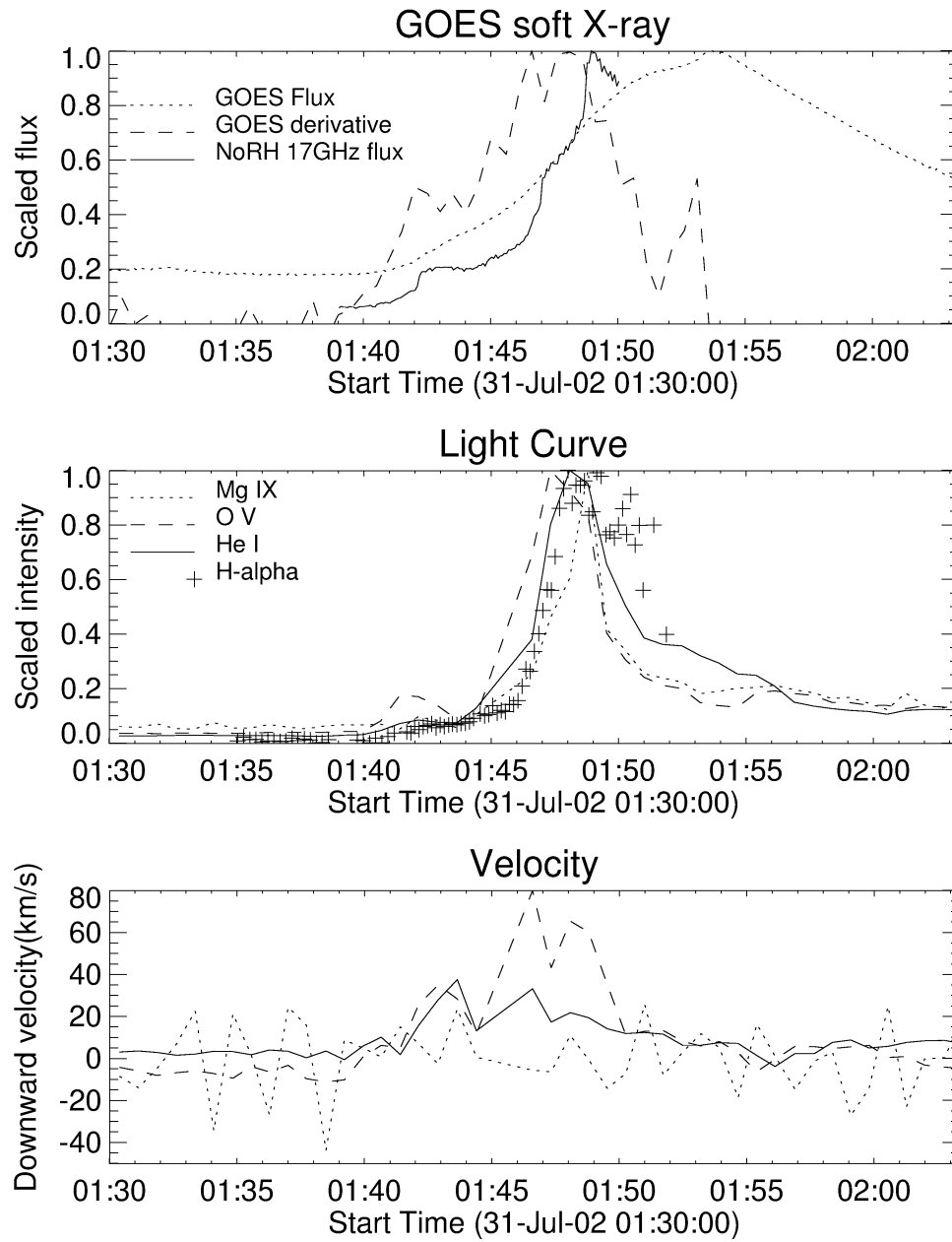


Figure 4. Same as Fig. 3, but for kernel A in the flare on 31 July 2002.

A TOPOLOGICAL ANALYSIS OF THE MAGNETIC BREAKOUT MODEL FOR AN ERUPTIVE SOLAR FLARE

Rhona Maclean⁽¹⁾, Colin Beveridge⁽²⁾, Dana Longcope⁽²⁾, Daniel Brown⁽¹⁾, and Eric Priest⁽¹⁾

⁽¹⁾*Institute of Mathematics, University of St Andrews, The North Haugh, St Andrews, Fife, KY16 9SS, UK*

⁽²⁾*Department of Physics, Montana State University, Bozeman, MT 59717-3840, USA*

ABSTRACT

The magnetic breakout model gives an elegant explanation for the onset of an eruptive solar flare. Reconnection at a coronal null point allows sheared, initially enclosed flux to “break out” explosively to large distances. We apply topological methods to evolutions of potential and linear force-free fields, in order to study magnetic configurations in which this type of breakout behaviour occurs. Rules are found governing the topological consequences of bifurcations between states, including the requirement that any new class of fieldlines must be created through a global topological bifurcation.

Key words: solar corona, solar flare, magnetic topology, magnetic breakout.

1. INTRODUCTION

Many explanations have been put forward for the onset of a solar flare. One of the most talked about in recent years has been the magnetic breakout model, as proposed by Antiochos, DeVore and Klimchuk (1999). In this model, a system of flux is initially enclosed by an overlying arcade. At a neutral line in the photosphere, shear is applied to the field. This causes reconnection to take place at a coronal null in the system, which in turn leads to a weakening of the overlying field. A critical point is reached at which the overlying field is no longer strong enough to hold down the central flux system; flux “breaks out” explosively, in a large-scale reconfiguration of the field topology.

On the Sun, the simplest magnetic configuration in which such a sequence of events can occur is a delta sunspot (Antiochos, 1998). A sunspot of this classification is formed when new flux emerges in the vicinity of a pre-existing simple sunspot, so that two opposite-polarity umbrae share a common penumbra. Indeed, delta sunspots are observed to be relatively prolific flare-producers (Tanaka, 1991), so the breakout explanation fits well.

The delta sunspot is modeled here according the principles of *magnetic charge topology* (MCT), which was first used by Longcope (1996). Its principal simplifying assumptions, justified in that paper, are that:

- Magnetic flux concentrations in the photosphere can be represented as point sources.

- These sources can be assumed to lie in the plane $z = 0$, representing the photosphere, with the corona considered to be the half-space $z > 0$.
- The magnetic field can be approximated by a potential or linear force-free field.

Assuming a potential field for now, an analytical expression for the magnetic field in the photosphere and corona from a given set of point sources can be found:

$$\mathbf{B}(\mathbf{r}) = \sum_{i=1}^n \epsilon_i \frac{\mathbf{r} - \mathbf{r}_i}{|\mathbf{r} - \mathbf{r}_i|^3}, \quad (1)$$

where \mathbf{r} is the point in space where the field is to be found, the \mathbf{r}_i are the source positions, and the ϵ_i are the source strengths.

Magnetic fields of this type have a complex structure, the elements of which have been extensively studied and catalogued. In particular, *null points* – points where the magnitude of the field vector is zero – are highly structured in 3D (Parnell *et al.*, 1996). Linearisation of the field near the null point leads to the identification of its *spine* fieldline and *fan plane*, associated with the eigenvectors of the linearised field. A null is classified as positive (negative) if its spine fieldlines connect to positive (negative) sources. Fan planes extend out to form *separatrix surfaces* which act as boundaries between the flux domains in a topology. Finally, *separators* are fieldlines which join two null points. Together, this set of null points and special fieldlines makes up the *skeleton* of the topology.

Changes to the structure of the skeleton, caused for example by altering the strength or position of a source, are called topological *bifurcations*. Two categories of bifurcation exist:

- *local* bifurcations in which the number of null points changes, and
- *global* bifurcations in which the structure of the field changes but the number of nulls is unaffected.

As various parameters in the delta sunspot model are altered, different bifurcations occur. We wish to find those bifurcations which cause the model to undergo the process of magnetic breakout.

| Source | Position | Strength |
|--------|----------------|------------|
| P1 | (0, 0) | ϵ |
| N1 | (0, 1) | -1 |
| N2 | (0.866, -0.5) | -1 |
| N3 | (-0.866, -0.5) | -1 |
| P2 | (0, -3) | 2.5 |
| P3 | (2.5, 1.5) | 2.5 |

Table 1. Initial source positions and strengths for our model

2. MODEL

The delta sunspot was modeled using six point magnetic sources on the photosphere plus a seventh balancing source at infinity. Table 1 gives the initial source configuration, which can also be seen as a plan view in the photosphere in Figure 1. The central source $P1$ represents the newly emerging flux, while the pre-existing simple sunspot is represented by positive sources $P2$ and $P3$, and negative sources $N1$, $N2$ and $N3$.

In this initial configuration, flux from $P1$ is prevented from connecting out to large distances by two separatrix domes; the separatrix of negative null $A1$, which touches the photosphere along the path $A1-P2-B1-P3-A1$, and the combined separatrices of positive coronal nulls $B2$ and $B3$, which touch the photosphere along the path $A2-N1-A4-N2-A3-N3-A2$. By altering parameters of the model, we hope to create breakout behaviour.

The topological manifestation of a breakout is the addition of a flux domain connecting the central, originally enclosed source to the balancing source at infinity. We shall attempt to provoke such behaviour by disturbing the configuration in three ways:

- by altering the strength ϵ of the central source in a potential field, from just above 0 up to 2;
- by altering the location of the central source in a potential field, within a 2×2 square centred on the origin; and
- by altering the parameter α of a force-free field, while keeping $P1$ fixed near the origin with $\epsilon = 1.5$.

The results of these three experiments are given in Section 4. First, we review some techniques for analysis of magnetic topologies.

3. ANALYSIS TECHNIQUES

There exist several rules and techniques which can assist with the analysis of complex topologies such as the ones studied here.

In the photosphere, the Euler characteristic equation relating the numbers of potential maxima, minima and sad-

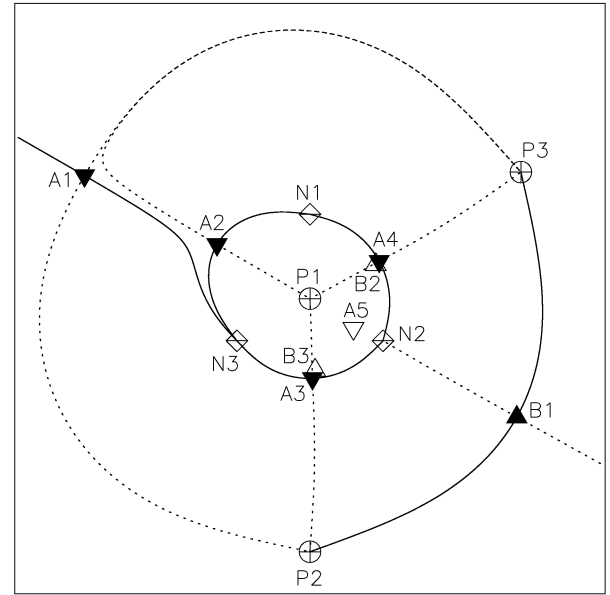


Figure 1. The initial state for our model, with the strength ϵ of the central source set equal to 1.5. The view here is the so-called ‘footprint’ of the topology, namely, a plan view of the fieldlines in the photosphere. Positive sources are circles (labeled P) and negative sources are diamonds (labeled N). Photospheric nulls are solid triangles, while coronal nulls are open triangles. The triangles for positive nulls (labeled B) point upwards, while those for negative nulls (labeled A) point downwards. Spines are indicated by continuous lines, and intersections of separatrix surfaces with the photosphere are dotted lines.

dle points becomes:

$$S + n_u = n_p + 2, \quad (2)$$

where S is the number of sources, n_u upright nulls (with spines normal to the photosphere), and n_p prone nulls (with spines tangent to the photosphere). In three dimensions, the relationship is:

$$S_+ - n_+ = S_- - n_-, \quad (3)$$

where S_{\pm} represents the number of positive or negative sources and n_{\pm} the number of positive or negative nulls. These Euler equations provide a check that any topology we calculate is self-consistent.

Further equations have been derived by Longcope and Klapper (2002) relating the various elements of the topology to one another. In particular, they found that in the photosphere and coronal half-space we can say:

$$D_{\phi} + 2D_c = 2X - n_{\phi} - 2n_c + S, \quad (4)$$

where D_{ϕ} is the number of photospheric domains (with some fieldlines in the photosphere), D_c the number of purely coronal domains (all fieldlines entirely in the corona and not the photosphere), n_{ϕ} the number of photospheric nulls and n_c the number of coronal nulls (Beveridge, 2003). This result excludes nulls both of whose

spines connect to the same null, and nulls with no separators.

Noting that neither the number of sources nor the number of flux domains changes in a local bifurcation, we can take the difference of Equation 4 before and after such a bifurcation to give:

$$\Delta X = \Delta n_c + \frac{1}{2}\Delta n_\phi \quad (\text{local bifurcation}), \quad (5)$$

which tells us how a local bifurcation changes the number of separators in a topology. Similarly, as a global bifurcation cannot change the number of nulls, Equation 4 reduces to:

$$\Delta X = \Delta D_c + \frac{1}{2}\Delta D_\phi \quad (\text{global bifurcation}). \quad (6)$$

Two further tools for our topological analysis are the domain and null graphs of a topology. The domain graph is constructed with the sources as its vertices, connected on the graph if they share flux. The null graph is constructed with the nulls as its vertices, connected on the graph if they share a separator. Changes to these graphs after a bifurcation can provide an accurate check on which type of bifurcation has taken place.

For example, a general rule can be outlined by which the global spine-fan bifurcation changes the null graph. A global spine-fan bifurcation involves the spine of one null, say S , passing through the fan of another null of the same sign, say T . We call this bifurcation $S \dashv T$. Let S' be the set of opposing null points connected directly to S by separators; let T' be those nulls connected to T prior to the bifurcation. The set \mathcal{U}' of null points which will be connected to T after bifurcation $S \dashv T$ is $\mathcal{U}' = (T' \setminus S') \cup (S' \setminus T')$. The bifurcation will destroy each separator connecting T to a member of $T' \cap S'$ while creating new separators connecting T to each member of $S' \setminus T'$.

It is thought that similar prescriptions exist for all the other types of bifurcation.

4. RESULTS

4.1 Changing Source Strength

Increasing the strength of the newly emerging flux $P1$ from just above 0 to 2 in relative units leads to an interesting sequence of topological bifurcations. Initially, when ϵ is very small, the flux from $P1$ is prevented from connecting out to large distances by the two separatrix domes described in Section 2.

The first bifurcation to take place is a coronal local separator bifurcation, which involves two separators in the corona – initially in a “V” configuration – being pushed together until they form a “Y”, with the creation of two new null points at the vertex of the “Y”. The two original separators are destroyed and four new ones are created. However, since this is a local bifurcation, it cannot create the new flux domain required for breakout.

The next bifurcation is a global spine-fan bifurcation, which turns out to be the bifurcation responsible for the breakout. Figures 2(a) and (b) show the topology before and after the bifurcation, which is $A5 \dashv A1$, occurring when ϵ passes 1.57. The spine of $A5$ and the separatrix of $A1$ pass through one another, causing the creation of a new flux domain linking $P1$ to N_∞ .

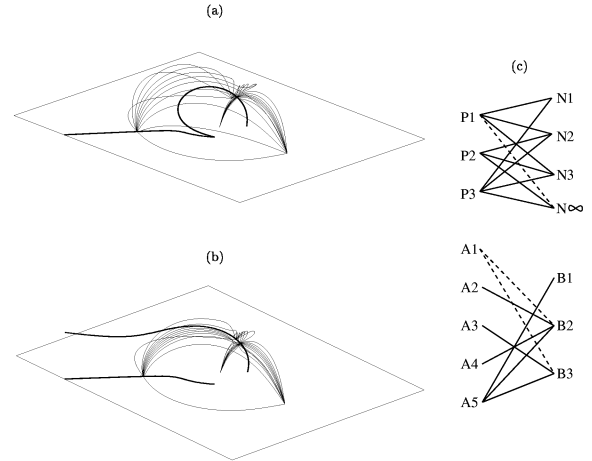


Figure 2. (a) A 3D view of the topology just before the global spine-fan bifurcation, when the spine (thick curve) of the coronal null connects down to the photosphere. (b) Once the bifurcation has taken place, the spine (thick curve) reaches out to infinity. A new coronal flux domain is created, connecting the central source to infinity. This is the breakout. (c) Domain graph (above) and null graph (below) after the global spine-fan bifurcation. New domains and separators created in the bifurcation are shown as dashed lines.

To find the change in connectivity brought about by the global spine-fan bifurcation, we apply our rule from Section 2. Here S is $A5$, T is $A1$, S' is $\{B1, B2, B3\}$ and T' is $\{B1\}$. So after the bifurcation, $A5$ should be connected to the set of nulls $\mathcal{U}' = (T' \setminus S') \cup (S' \setminus T')$, which here is $\{B2, B3\}$. This can be seen in the new domain and null graphs, given in Figure 2(c).

We also need to check that equation 6 is still satisfied after this global bifurcation; we have $\Delta D_c = 1$, which is balanced by the fact that on the other side $\Delta X = 1$, so the equation is indeed satisfied.

A final point to note regarding this topology is that, according to Longcope and Klapper (2002), a coronal domain such as the one produced by the global spine-fan bifurcation must be enclosed by a *separator circuit*. Prior to the global spine-fan bifurcation there were no separator circuits and therefore no coronal domains. The post-bifurcation null graph (Figure 2(c)), with $X = 7$ separators and $n = 7$ nulls, contains $X - n + 1 = 1$ separator circuit. This circuit is $A1-B2-A5-B3-A1$, as can be seen on Figure 2(c); it engirdles the new domain $P1-N_\infty$ as anticipated.

As the strength of $P1$ continues to increase, further bi-

furcations are observed. However, flux in the breakout domain continues to increase, until we can safely conclude that no possible bifurcation could feasibly reverse the breakout process.

4.2 Changing Source Position

In the second experiment in the attempt to provoke breakout behaviour in the model delta sunspot, the strength of the central source $P1$ was fixed at $\epsilon = 1.5$. Instead, the position of the source was altered, the source being moved around inside a 2×2 box centred on the origin. This scenario does not allow us to define a sequence of bifurcations as in Section 4.1; rather, as we will see, breakout is observed in many distinct directions as $P1$ moves around the photosphere.

Figure 3 shows the bifurcation diagram generated by this experiment. It is almost symmetrical due to the arrangement of sources chosen. Shading shows where breakout topologies can be found; it is interesting to note that moving in many directions from the origin leads to breakout. In fact if the source is moved far enough out in any direction, breakout will eventually occur.

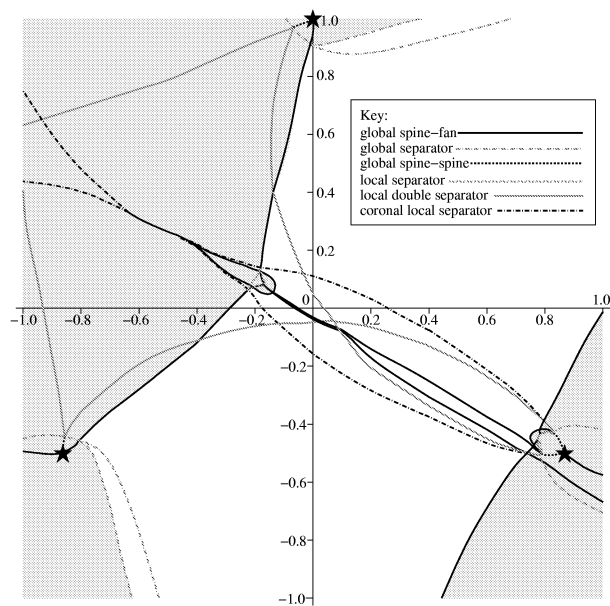


Figure 3. Bifurcation diagram created by varying each of the coordinates of the central source in the photosphere between $+1$ and -1 . Shaded areas show where breakout topologies occur.

As can be seen in Figure 3, two different types of bifurcation can cause breakout in this scenario – the global spine-fan bifurcation as before, and also the global separator bifurcation. The global separator bifurcation involves two separatrix surfaces being pushed together until they pass through one another and the connectivity changes.

Figure 4 shows an example of the global spine-fan bifurcation causing breakout, taken from moving across the

global spine-fan bifurcation line on the bifurcation diagram at approximately $(0.9, -0.2)$. As all the nulls are prone, the topology can be described completely through study of its photospheric footprint.

The actual bifurcation is the global spine-fan bifurcation $B1 \rightarrow B2$, proceeding as follows. As $P1$ moves further right across the photosphere, the spine $B1-P3$ and the separatrix $B2-N2$ are pushed closer and closer together, until they coincide at about $x = 0.9$ in a global spine-fan bifurcation. After the bifurcation, the spine connects $B1-P1$ and the separatrix $B2-N\infty$.

We apply our separator rule to find changes to the topological structure; here, with $B1$ as S and $B2$ as T , we see that $S' = \{A1, A3\}$ and $T' = \{A2, A3\}$, giving $U' = \{A1, A2\}$. So the number of separators before and after the bifurcation is constant at $X = 5$. Putting this into equation 6 tells us that, as there are no coronal domains, the number of photospheric domains should remain unchanged. This is indeed the case; the bifurcation destroys the flux domain $P3-N2$, while at the same time creating a new flux domain $P1-N\infty$, the breakout domain.

Now we study an example of the global separator bifurcation causing breakout, taken from crossing the line of bifurcation at approximately $(0.2, 0.95)$. Again, the photospheric footprint completely specifies the topology.

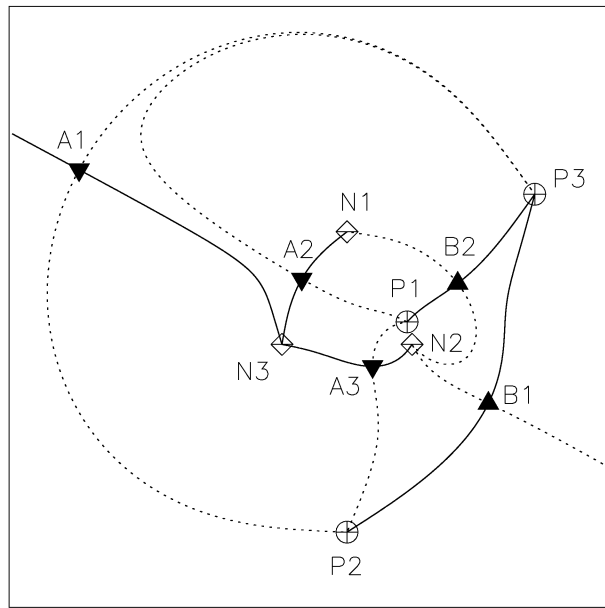
As $P1$ moves up, the separatrices $B2-N3$ and $A1-P3$ are pushed closer together. At the point of bifurcation they coincide, and then, as $P1$ continues to move, the breakout takes place and the flux domain $P1-N\infty$ is created. The separatrices involved in the bifurcation change connectivity; they now join $B2-N\infty$ and $A1-P1$.

Equation 6 applies as we are dealing with a global bifurcation. This time we have $\Delta X = 1$ as a new separator, $A1-B2$, is created. The equation holds, because $\Delta D_c = 1$ as flux domain $P3-N3$ is pushed up into the corona by the bifurcation, changing its classification from photospheric to coronal. $\Delta D_\phi = 0$ because the creation of the (photospheric) breakout domain $P1-N\infty$ balances the loss of the domain $P3-N3$ to the corona.

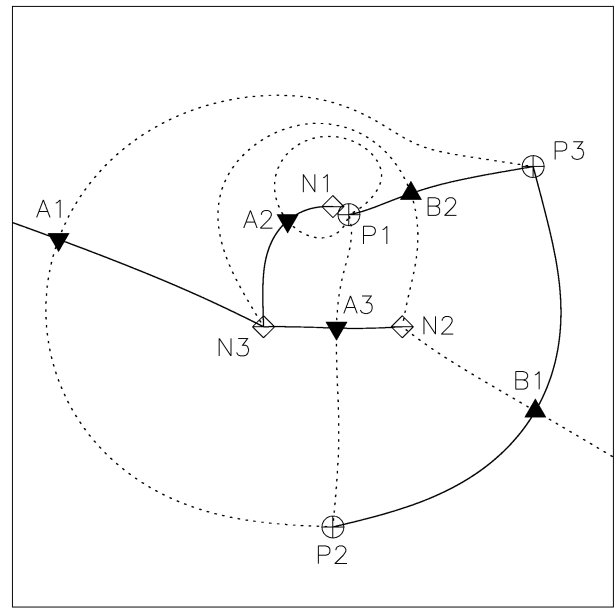
4.3 Changing Force-Free Parameter α

In this third and final experiment, the central source $P1$ is fixed in both position (at $(-0.05, 0.05)$) and strength (at 1.5), and instead the value of the force-free parameter α is altered. The contribution to the field from each source is given by a Green function (Chiu and Hilton, 1977); we can sum over all the sources to find the field for a given value of α . The only restriction on the use of linear force-free fields is that at a radius greater than $\pi/2|\alpha|$ the elsewhere radial field begins to oscillate in space. Therefore we restrict our attention to the field inside this radius, and refer to fieldlines leaving the region as extending to “infinity”.

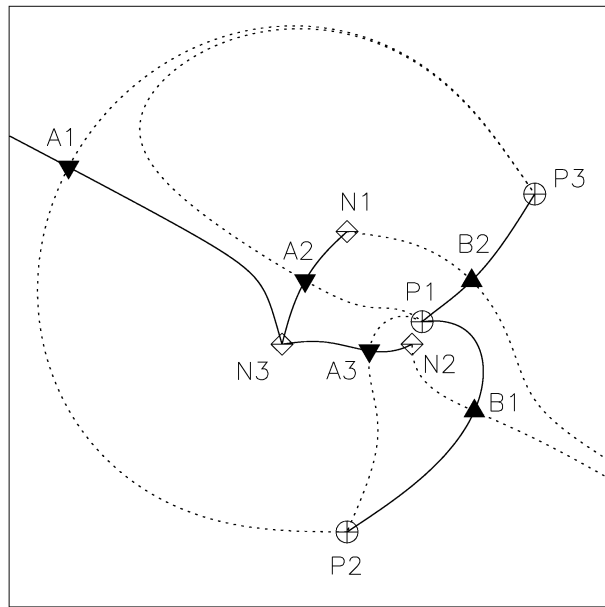
Starting with $\alpha = 0$, we allow the value of α to decrease and observe the sequence of bifurcations which follows.



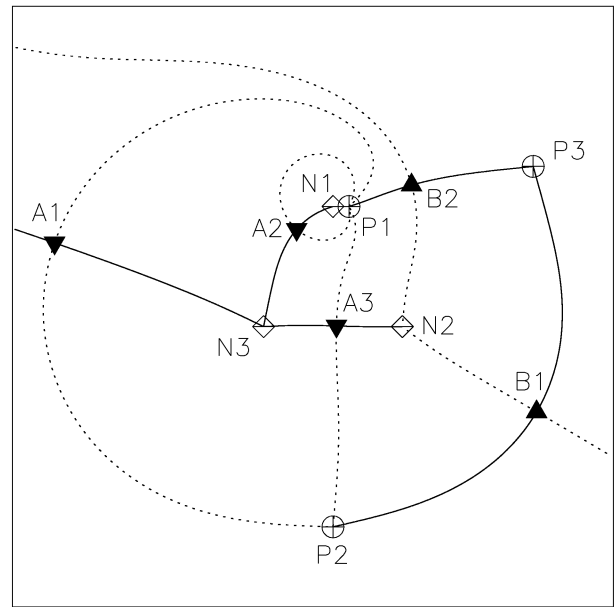
(a)



(a)



(b)



(b)

Figure 4. An example of the global spine-fan bifurcation causing breakout. The footprints are shown when the central source is at (a) $(0.8, -0.2)$, before the global spine-fan bifurcation and (b) $(1.0, -0.2)$, after the bifurcation. The upper spine of B1 changes its connection from P3 to P1, while the lower fan trace of B2 changes its connection from N1 to N_∞ .

Figure 5. An example of the global separator bifurcation causing breakout. The footprints are shown when the central source is at (a) $(0.2, 0.9)$, before the global separator bifurcation and (b) $(0.2, 1.0)$, after the bifurcation. The upper fan trace of A1 changes its connection from P3 to P1, while the upper fan trace of B2 changes its connection from N3 to N_∞ .

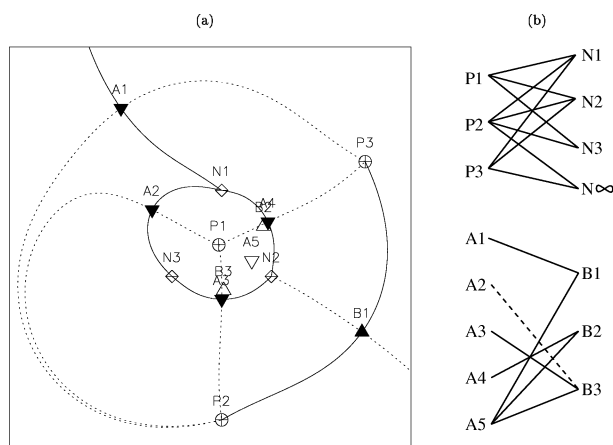


Figure 6. (a) The footprint of the force-free field $\alpha = -0.1$ with $\epsilon = 1.5$, and source $P1$ at $(-0.05, 0.05)$. (b) Domain and null graphs for this topology.

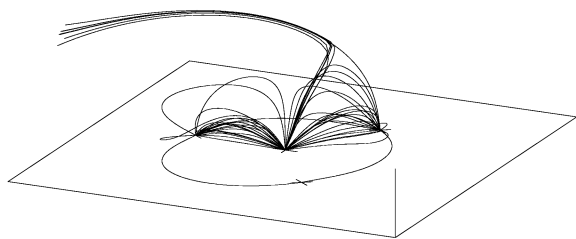


Figure 7. Field lines from a force-free field with the same source configuration as previously, but $\alpha = -0.21$; beyond the breakout bifurcation. Lines in the photosphere are the spines of the photospheric nulls $A1$, $A2$ and $A3$. The field lines which close down to the photosphere are from domains $P1-N2$ and $P1-N3$. The field lines which extend out of the diagram to the top left are from $P1-N\infty$, the flux domain created by breakout.

In fact, this consists of three global spine-fan bifurcations at $\alpha = -0.011$, -0.028 and -0.197 , with the third bifurcation being the one which causes breakout. Figure 6 shows the footprint of the topology just before the breakout bifurcation.

The third global spine-fan bifurcation is $A5 \rightarrow A1$, taking the spine of $A5$ to “infinity” (i.e. beyond $r \simeq 7.5$). The bifurcation destroys separator $A1-B1$, and creates separators $A2-B1$ and $A3-B1$ ($\Delta X = 1$). This forms a separator circuit $A2-B2-A3-B3-A2$ engirdling a new coronal domain, $P1-N\infty$, which is the breakout domain. Figure 7 shows field lines, for $\alpha = -0.21$, from the breakout domain and two of the domains which had been under the dome prior to breakout.

The manner in which the breakout proceeds is very similar to the previous potential field calculations, suggesting that a potential field gives a good qualitative picture of the topological behaviour of our sunspot.

5. CONCLUSIONS

The magnetic breakout model as established by Antiochos, DeVore and Klimchuk (1999) is in essence a dynamic model, and as such a topological study cannot hope to capture all of its features, especially with regard to energy considerations. However, even a simple potential field model such as the one developed here is capable of showing topological breakout behaviour. Somewhat more complex linear force-free fields can also exhibit this phenomenon.

Breakout has been defined in this context as the creation of a new class of fieldlines (flux domain) linking newly emerging flux in the photosphere out to large distances. Only global bifurcations can cause this type of behaviour, as only they are capable of changing the field connectivity in such a way as to create this new flux domain. Here we have seen examples of this happening due to both the global spine-fan bifurcation and the global separator bifurcation.

It has been shown that breakout can be provoked by increasing the strength of newly emerging flux, changing its location on the photosphere, or adding twist to the field by changing the force-free parameter α . In fact, it seems that breakout behaviour is ubiquitous in our delta sunspot model; whichever parameter is varied, the system can eventually make its way towards a breakout configuration.

We hope that this work will pave the way for more realistic topological simulations of the magnetic breakout model.

ACKNOWLEDGEMENTS

We are grateful to the UK Particle Physics and Astronomy Research Council for funding.

REFERENCES

- Antiochos, S. K., 1998, *Astrophys. J.* **502**, L181–L184
- Antiochos, S. K., DeVore, C. R. and Klimchuk, J. A., 1999, *Astrophys. J.* **510**, 485–493
- Beveridge, C., 2003, Ph.D. thesis, University of St. Andrews
- Chiu, Y. T. and Hilton, H. H., 1977, *Astrophys. J.* **212**, 873–885
- Longcope, D. W., 1996, *Solar Phys.* **169**, 91–121
- Longcope, D. W., 2001, *Physics of Plasmas* **8**, 5277–5290
- Longcope, D. W., and Klapper, I., 2002, *Astrophys. J.* **579**, 468–481
- Parnell, C. E., Smith, J. M., Neukirch, T. and Priest, E. R., 1996, *Phys. Plasmas* **3**, 759–770
- Tanaka, K., 1991, *Solar Phys.* **136**, 133–149